

RSC Advances



This is an *Accepted Manuscript*, which has been through the Royal Society of Chemistry peer review process and has been accepted for publication.

Accepted Manuscripts are published online shortly after acceptance, before technical editing, formatting and proof reading. Using this free service, authors can make their results available to the community, in citable form, before we publish the edited article. This *Accepted Manuscript* will be replaced by the edited, formatted and paginated article as soon as this is available.

You can find more information about *Accepted Manuscripts* in the [Information for Authors](#).

Please note that technical editing may introduce minor changes to the text and/or graphics, which may alter content. The journal's standard [Terms & Conditions](#) and the [Ethical guidelines](#) still apply. In no event shall the Royal Society of Chemistry be held responsible for any errors or omissions in this *Accepted Manuscript* or any consequences arising from the use of any information it contains.

1Chitosan modification of magnetic biochar produced from
2*Eichhornia crassipes* for enhanced sorption of Cr(VI) from
3aqueous solution

4Ming-ming Zhang^{a,b}, Yun-guo Liu^{a,b*}, Ting-ting Li^{a,b}, Wei-hua Xu^{a,b}, Bo-hong Zheng^c,
 5Xiao-fei Tan^{a,b}, Hui Wang^{a,b}, Yi-ming Guo^d, Fang-ying Guo^{a,b}, Shu-fan Wang^{a,b}

6^a College of Environmental Science and Engineering, Hunan University, Changsha
 7410082, PR China

8^b Key Laboratory of Environmental Biology and Pollution Control (Hunan
 9University), Ministry of Education, Changsha 410082, PR China

10^c School of Architecture and Art Central South University, Changsha 410082, PR
 11China

12^d School of Economics and Management, Shanghai Maritime University, 1550
 13Haigang Ave, Shanghai 201306, PR China

14
 15
 16
 17
 18
 19
 20
 21

1* Corresponding author at: College of Environmental Science and Engineering, Hunan University, Changsha
 2410082, PR 9 China. Tel.: + 86 731 88649208; Fax: + 86 731 88822829; E-mail address:
 3hnyliuyunguo@hnu.edu.cn

Abstract

In this research, chitosan modification of magnetic biochar (CMB) was successfully prepared for effective removal of Cr(VI). Moreover, this study highlighted that the conversion of *Eichhornia crassipes* into biochar was a promising method for improved management of this highly problematic invasive species. The sorption kinetics, isotherms, thermodynamics, the effects of pH, and background electrolyte on the sorption process were investigated. The results indicated that CMB adsorbed more Cr(VI) (120 mg g^{-1}) than that of pristine biochar (30 mg g^{-1}). The sorption data could be well illustrated by pseudo-second-order and Langmuir models. Furthermore, thermodynamic parameters revealed that the sorption reaction was an endothermic and spontaneous process. The adsorption of Cr(VI) was influenced by solution pH and the maximum sorption capacity was achieved at pH 2. The background electrolyte PO_4^{3-} and SO_4^{2-} restricted the Cr(VI) sorption. These results are significant for exploring and optimizing the removal of metal ions by CMB composite.

Keywords: Chitosan, Magnetic biochar, Hexavalent chromium, Modification, Adsorption

1 Introduction

Chromium is one of the most widespread heavy metals in the environment. However, chromium is also considered to be a major pollutant, even a priority pollutant, by the US EPA.¹ Because Cr(VI) is highly carcinogenic after long-term or

43high-dose exposure, Cr(VI) pollution of soil and water can pose a great threat to public
44health.² Therefore, it is urgent and necessary to take efficient measures to dispose the
45wastewater containing high concentration of Cr(VI). Up to now, various technologies
46have been employed for Cr(VI) removal, such as ecological remediation,³ chemical
47precipitation,⁴ redox,⁵ and adsorption.⁶ Among these techniques, adsorption is regarded
48as the most effective and common method to remove Cr(VI) from wastewater. A
49variety of adsorbing materials have been applied for Cr(VI) removal through
50experiment, such as biochar, chitosan,⁷ iron oxide.⁸

51 *Eichhornia crassipes*, a tropical species, is one of the pickerelweed family
52(Pontederiaceae). It has been characterized as one of the 100 most aggressive invasive
53species by IUCN (the International Union for Conservation of Nature) and one of the
54top 10 worst weeds globally.⁹ *Eichhornia crassipes* grows and reproduces rapidly,
55leading to navigation jam, interference with irrigation, fishing and power generation.¹⁰
56In addition, *Eichhornia crassipes* can block sunlight penetration, reduce the DO
57concentration of water, competitively exclude submerged plants, and reduce
58biodiversity.¹¹ As a result, the conversion of *Eichhornia crassipes* into biochar
59afterwards application in the removal of Cr(VI) from waste water may represent a
60novel and attractive method for managing and controlling this highly problematic
61invasive species effectively.

62 Biochar, the product of *Eichhornia crassipes* through pyrolysis, has drawn much
63experiment attention recently due to its potential in resource reuse and soil
64improvement as well as providing renewable bioenergy and mitigating global climate

change. Biochar is a stable solid, rich in carbon, and can sequester carbon in soils for thousands of years.¹² Moreover, recent studies also find biochar can be used as a low-cost sorbent to remove various contaminants from water.¹³ The large specific surface area, porous structure, enriched surface functional groups and mineral components of biochar make it possible to be used as proper adsorbent to remove pollutants from aqueous solutions.¹⁴ However, pristine biochars prepared from biomass feedstock without any treatment have relatively low heavy metal sorption capacity.¹⁵ Therefore, various modification/activation methods, such as surface oxidization, exploration, and functionalization, have been applied to improve their performance in environmental remediation.¹⁶⁻¹⁸ As previously mentioned, these modifications can add the surface sorption sites, introduce more positive charges and surface functional groups on the modified surfaces, which is vital for the sorption of Cr(VI) by biochar.^{2, 15} Nowadays, various methods have also been developed to change the characteristics of biochar surfaces and improve their sorption ability.

Chitosan has been intensively studied previously. It is abundant, renewable, biodegradable and non-toxic in nature. Recently, chitosan has been applied to water purification and removing heavy metals from aqueous solutions.¹⁵ It has also been used as a surface modification agent impregnated onto supporting surfaces as adsorption sites because its amine functional groups have strong bonding ability to various heavy metal ions.^{15, 19} So far, the research on the use of chitosan to modify the surfaces of biochars to enhance their affinity to heavy metal is limited. This combination is promising and it make full use of the advantages of biochar and

87chitosan, which is beneficial to bond Cr(VI).

88 Although the chitosan-modified biochar exhibited good sorption ability, it is
89difficult to be separated from aqueous solution. Therefore, an easy separation
90approach should be taken into account. Since exhausted biochar-based adsorbent may
91contain a good deal of pollutants when it is applied to treat natural water bodies. It is
92necessary to develop a technique to collect the pollutant-laden adsorbents from
93aqueous solutions to avoid secondary pollution. γ -Fe₂O₃ particles have high utility
94value in wastewater purification considering their low cost and easy separation. They
95have been successfully applied to remove organic contaminants,²⁰ and heavy metals ²¹.
96However, due to their high surface energy arising from strong van der Waals forces,
97the γ -Fe₂O₃ nanoparticles have a tendency to form aggregates in aqueous solutions,
98which dramatically decrease the surface area and adsorption abilities as well as
99increase the cost.²² In order to bring out the potentials of the chitosan-modified
100biochar and the γ -Fe₂O₃ nanoparticles, we immobilized the γ -Fe₂O₃ nanoparticles into
101the biochar-based adsorbent.^{1, 23} So chitosan-biochar/ γ -Fe₂O₃ could be produced to not
102only enhance the sorption ability but also be magnetically collected after use.

103 In this study, chitosan-modified magnetic biochars were synthesized and used to
104remove Cr(VI) successfully. The prepared material was characterized by scanning
105electron microscopy (SEM), Fourier transform infrared (FTIR) analysis, X-ray
106photoelectron spectroscopy (XPS) analysis, (Brunauer–Emmett–Teller) BET analysis.
107Moreover, the relevant parameters such as pH, kinetics, and sorption isotherms were
108investigated to study the adsorption property of chitosan-modified magnetic biochars

109for Cr(VI) in aqueous solution. In addition, the competitive adsorption of the [ion](#)
110[strength](#) in the presence of various background electrolyte ions was also verified.

1112 Materials and methods

1122.1 Materials

113 Ferric chloride-6-hydrate ($\text{FeCl}_3 \cdot 6\text{H}_2\text{O}$) were purchased from Tianjin Kermel
114Reagent Co. Ltd., Tianjin, China. Chitosan (90% acetylation degree) was supplied by
115Sinopharm Chemical Reagent Co. Ltd., Shanghai, China. Glutaraldehyde was
116provided by Tianjin Guangfu Fine Chemical Research Institute, Tianjin, China. All
117reagents used in the experiment were of analytical reagent grade and solutions were
118prepared with high-purity water ($18.25 \text{ M}\Omega \text{ cm}^{-1}$) from Millipore Milli-Q water
119purification system. The pristine biochar was produced from *Eichhornia crassipes*.

1202.2 Preparation of biochar and biochar/ $\gamma\text{-Fe}_2\text{O}_3$ composite

121 The biomass, *Eichhornia crassipes*, was dried and smashed. The treated biomass
122was divided into two-part. One part was immersed into the prepared FeCl_3 solution
123for 24 h. The mixture was oven-dried (80°C). Both the FeCl_3 treated biomass and the
124pristine *Eichhornia crassipes* were pyrolyzed in a tube furnace at 600°C in N_2
125environment for 1 h. The product of non-treated biomass and pre-treated biomass
126were henceforth referred to as B, MB, respectively. The samples were then washed,
127dried (80°C), and sieved through 100 mesh screen. At last, they were sealed to
128preserve before use.

1292.3 Preparation of chitosan-biochar/ γ -Fe₂O₃ composite

130 6 g of chitosan was first dissolved in 1000 mL of 2% (v/v) acetic acid.
131 Afterwards, 6 g of biochar/ γ -Fe₂O₃ composite was added and the compounds were
132 stirred for 30 min at 40 °C. 150 mL glutaraldehyde (1% v/v) was then injected into the
133 reaction system. After 30 min, keeping in 40 °C, NaOH solution was added dropwise
134 into the mixtures until the pH value reached 9. In the end, the compounds were also
135 stirred for 1 h. The detailed preparation process was shown in Fig. 1. The final
136 product was chitosan-biochar/ γ -Fe₂O₃ composite (CMB).

1372.4 Materials characterization

138 Scanning electron microscope (SEM) images were obtained on a JEOL JSM-
139 6700. FT-IR spectrum was measured on a spectrophotometer (Varian 3100, USA)
140 using the KBr pellet technique. The XPS measurements were performed using an
141 ESCALAB 250Xi X-ray photoelectron spectrometer (Thermo Fisher, USA). BET
142 analysis was carried out with Tristar II 3020 (USA). The magnetic property was
143 characterized by magnetization curve using a vibrating sample magnetometer (Lake
144 Shore 7410, USA). The zeta potentials of CMB were measured at different pH by
145 Zetasizer Nano ZS (ZEN3690, Malvern, UK).

1462.5 Sorption experiments

147 All batch sorption experiments were carried out in a 150 mL Erlenmeyer flask
148 containing 50 mL Cr(VI) solutions in an incubator shaker with a shaking speed of 150

149rpm. For each treatment, 50.0 mg of adsorbent was added and shaken for specified
150period. The concentrations of residual Cr(VI) were determined by UV-vis
151spectrophotometer (Pgeneral T6, Beijing, China) at 540 nm.

152 Three kinds of adsorbents (B, MB, CMB) were used to study the effect of pH on
153Cr(VI) ions adsorption. Effects of pH (2.0–8.0) experiments were studied in 50 mL
154Cr(VI) solutions with the initial Cr(VI) concentration of 150 mg L⁻¹ at 30 °C. The pH
155was adjusted to desired values by adding negligible volumes of NaOH or HCl.

156 Isotherm experiments were conducted with different initial Cr(VI) concentrations
157(20–500 mg L⁻¹) for 24 h. The experiments were carried out at different temperatures
158of 20, 30 and 40 °C, respectively.

159 Kinetic experiments were studied for different time intervals (5, 10, 30, 60 min
160and 2, 6, 12, 18, 24 h) 30 °C. In each study, 50.0 mg CMB was added to 50 mL
161Cr(VI) solution with the initial concentration of 200 mg L⁻¹.

162 The adsorption amount q_e (mg g⁻¹) of Cr(VI) was calculated according to Eq. (1)

$$163 q_e = \frac{(c_0 - c_e) \times V}{m} \quad (1)$$

164where c_0 and c_e were the initial and residual concentration of Cr(VI) in the solution
165(mg L⁻¹), respectively. V is the volume of Cr(VI) solution (mL), and m is the amount
166of adsorbent used (mg).

1673. Results and discussion

1683.1. Characterization of B, MB, CMB

169 The surface morphologies of the pristine biochar (B), magnetic biochar (MB)
170and chitosan-biochar/ γ -Fe₂O₃ (CMB) were displayed in the SEM images. As shown in
171the Fig. 2 (a), the pore structure of the pristine biochar surface was un conspicuous.
172However, after being disposed by FeCl₃, the biochar surface morphology formed
173plenty pore channels apparently, as displayed in Fig. 2 (b). Besides, some splendid
174particles appeared on the surface of MB, and it may be γ -Fe₂O₃.²² Fig. 2 (c) showed
175the pore amount decreased distinctly. This phenomenon was explained that the
176biochar/ γ -Fe₂O₃ was modified by coating chitosan onto it and the chitosan blocked the
177pore channel. Nevertheless, the sorption capacity of CMB was stronger than that of
178MB, which indicated that the adsorption mechanism relied on the functional groups
179primarily but not the surface pore structure.

180 The FTIR spectra of B, MB, CMB were shown in Fig. 3 (a). For CMB, the peak
181around 3419 cm⁻¹ was related to the stretching vibration of -OH and -NH groups.^{24, 25}
182The characteristic peak of CMB at 2917.5 cm⁻¹ was attributed to the stretching
183vibration of -CH and -CH₂. The adsorption band at 1687.5 cm⁻¹ was corresponded to
184the C=O stretching vibrations of -NH-C=O from chitosan or the carbonyl from the
185carboxyl group in biochar.^{19, 24, 26} The band at 1073.5 cm⁻¹ may be connected with the
186C-O stretching vibration from chitosan. For CMB and MB spectra, the peaks at 576.4
187and 576.8 cm⁻¹ were found obviously, which was assigned to Fe-O stretching
188vibration. It indicated that γ -Fe₂O₃ particles were embedded in the pristine biochar. It
189can be observed notably from Fig. 3 (a) that the types of functional groups of CMB

190 were much more than that of pristine material. The FTIR spectra of B, MB, CMB
191 were different with each other, which can account for the distinction of the sorption
192 capacity of the three materials for Cr(VI) to some extent.

193 The FTIR spectra of CMB before and after Cr(VI) adsorption was shown in Fig.
194 (b). After adsorption, a significant shift of those peaks (CMB) from 3419 cm^{-1} (-OH
195 & -NH) to 3413.1 cm^{-1} , 1687.5 cm^{-1} (C=O of -NH-C=O) to 1589.6 cm^{-1} , and 1073.5
196 cm^{-1} (C-O) to 1064.2 cm^{-1} occurred perhaps. This result indicated that the main
197 mechanism of Cr(VI) adsorption onto CMB may rely on the functional groups on the
198 material surface.

199 With the purpose of gaining further information on the chemical composition of
200 biochar and chitosan-biochar/ $\gamma\text{-Fe}_2\text{O}_3$, X-ray photoelectron spectroscopy (XPS) was
201 performed to examine the surface chemical ingredients of two materials, and the
202 results were exhibited in Fig. 4 (a) and Fig. 5 (a), (b). In the XPS survey of B, three
203 significant peaks C 1s (78.87%), O 1s (19.51%) and N 1s (1.62%) were observed. In
204 addition to these three peaks, Fe 2p was presented in the XPS survey spectra of CMB,
205 and the four peaks were shown as follows: C 1s (71.24%), O 1s (23.02%), N 1s
206 (3.2%) and Fe 2p (2.54%). Comparing the two XPS survey spectra, the O/C atomic
207 ratio and the amount of N 1s of CMB were higher than that of B, both of which were
208 owing to the introduction of chitosan to $\gamma\text{-Fe}_2\text{O}_3$ /biochar thus leading to the increase in
209 the amount of oxygenic groups. Moreover, the existence of iron indicated that the
210 preparation of $\gamma\text{-Fe}_2\text{O}_3$ /biochar composite was successful. Fig. 5 (a) expressed the C
211 1s XPS spectra of B, which demonstrated a considerable degree of oxidation with four

212 components corresponding to carbon atoms in different functional groups: non-
213 oxygenated ring C (284.5 eV), the carbon in the C-O (286.1 eV), C-N (285.2 eV) and
214 COOH groups (290 eV).^{27, 28} For Fig. 5 (b), the C 1s XPS spectra of CMB included
215 four peak components too, but it represented 284.6, 286.1, 287.5, 288.7 eV, consistent
216 with C-C, C-O, C-N, and -COOH, respectively.^{29, 30} The difference of the two C 1s
217 XPS spectra was possibly due to the modification of biochar using chitosan and ferric
218 chloride solution.

219 Fig. 4 (b) showed the XPS survey spectra of CMB before and after Cr(VI)
220 adsorption. After adsorption, a new typical peak at the binding energy of 586.6 eV
221 corresponding to Cr(VI) ions appeared,³¹ which provided testify further that the
222 process of Cr(VI) ions adsorption onto CMB took place.

223 Fig. 5 (c) represented the C 1s XPS spectra of CMB after Cr(VI) adsorption.
224 After Cr(VI) adsorption, there were four peaks appeared in the C 1s XPS spectra of
225 CMB, and they were C-C (283.8 eV), C-N (285.6 eV), C-Cr (287.1 eV) and
226 $[\text{Cr}(\text{CO})_6]$ (287.9 eV). Apparently, compared with the C 1s XPS spectra of CMB
227 before adsorption (Fig. 5 (b)), the carbon functional groups of CMB changed greatly
228 after Cr(VI) adsorption. That is to say the carbon functional groups was the main
229 adsorption mechanism.

230 As shown in Table 1, the surface area, pore volume and pore size of B, MB and
231 CMB existed distinction. The BET surface area of MB ($341.09 \text{ m}^2 \text{ g}^{-1}$) was larger than
232 that of B ($37.68 \text{ m}^2 \text{ g}^{-1}$), and the MB possessed larger pore volume and smaller pore
233 size than that of B. The phenomenon may be due to the process of preparing γ -

234Fe₂O₃/biochar, which was manufactured by immersing water hyacinth biomass into
235ferric chloride solution, and then changed the pore structure of pristine biochar.
236Compared with MB, CMB owned smaller BET surface area and pore volume, but
237bigger pore size, which resulted from coating chitosan on the surface of γ -
238Fe₂O₃/biochar and the pore channels of MB was clocked. Nevertheless, the adsorption
239activity of the CMB was greater than MB. These results suggested that the main
240mechanism for heavy metal adsorption on the CMB was not the pore structure but the
241surface functional group,³² which is consistent with the SEM analysis partially.

242 The room-temperature magnetization hysteresis curve was measured using
243vibrating sample magnetometry (VSM) to study the magnetic properties of CMB. As
244shown in Fig. 6, the magnetic hysteresis loop was S-like curve. The saturation
245magnetization (M_s) of the CMB composite was 11.60 emu g⁻¹, which was sufficient to
246be separated from aqueous solution by a permanent magnet. The insets in Fig. 6
247showed that the obtained CMB can be collected by a permanent magnet from aqueous
248solution. The result confirmed that CMB was magnetic and can potentially be used as
249an magnetic adsorbent to remove pollutants in liquidphase processes.

2503.2. Effect of initial solution pH

251 The initial solution pH is a significant factor in sorption process. The removal
252tendencies of Cr(VI) by CMB, MB and B under different initial solution pH were
253presented in Fig. 8 From Fig. 8, the sorption capacities of CMB, MB and B for Cr(VI)
254reduced gradually with the increase of pH from 2.0 to 8.0, and the adsorption amount

reached the maximum value at pH 2.0. The pH dependence of Cr(VI) was largely connected with the speciation of Cr(VI) and the surface charge of the sorbents.²⁸ Cr(VI) existed in different forms in aqueous solution at different pH values, such as H_2CrO_4 (aq), $\text{Cr}_2\text{O}_7^{2-}$, HCrO_4^- , KCrO_4^- , CrO_4^{2-} . HCrO_4^- is the predominant Cr(VI) species at $\text{pH} < 6.51$, while CrO_4^{2-} was predominant at $\text{pH} > 6.51$.²⁸ That is to say the main speciation of Cr(VI) ions is anionic. The zeta potentials of CMB at different pH values were shown in Fig. 7. The zero point of zeta potential (pH_{ZPC}) for CMB was at pH 6.19. When the solution $\text{pH} < \text{pH}_{\text{ZPC}}$, the hydrated surface of CMB was protonated, which made the CMB surface potential electropositive. As a result, a remarkable electrostatic attraction occurred between the positively charged surface of the sorbent and the anionic Cr(VI) ions, which contributed to the high adsorbing capacity of Cr(VI) ions onto CMB. Nevertheless, under the solution $\text{pH} > \text{pH}_{\text{ZPC}}$, with the increasing of pH value, the hydrated surface of CMB was deprotonated. It caused the sorbent acquired a negative charge, which generated electrostatic repulsion that made the sorbent surface site reject the anionic Cr(VI) ions. Moreover, at $\text{pH} > \text{pH}_{\text{ZPC}}$, the OH^- was abundant in the solution, which can compete with Cr(VI) ions for the available adsorption sites on the surface of CMB. These are the reasons for the decrease of sorption capacity at higher pH.

From Fig. 8, we can see that the adsorption capacity of the above three materials were discrepant ($\text{CMB} > \text{MB} > \text{B}$). Compared with B, it was more effective for MB to eliminate Cr(VI) within a wide pH range. This could be due to the conjuncture of Cr(VI) adsorption and an Fe-Cr complex reaction,¹ which lowered the

concentration of Cr(VI) in the solution. Besides, the sorption capacity of CMB was higher than that of MB. The reason was that the chitosan modification introduced -NH₂. In environment of pH < 6, -NH₂ was protonated resulting in a stronger attraction for anionic Cr(VI) ions. The visual sorption process was displayed in Fig. 1. Moreover, in acidic environment, -COOH may be protonated, which also enhanced the sorption of anionic Cr(VI) ions on CMB. In conclusion, the new adsorbent was more effective than the pristine material on adsorbing Cr(VI) ions.

3.3. Adsorption isotherm

The sorption isotherms of Cr(VI) on the CMB were presented in Fig. 9, which showed that the adsorption capacities increased with the increasing of equilibrium concentrations, and finally approached the maximum adsorption capacities. Besides, when the initial concentration was lower than 20 mg L⁻¹, the residual Cr(VI) in the solution after adsorption by the CMB was negligible. In this study, Langmuir and Freundlich models were adopted to simulate the experimental data, and thus described the adsorption characteristics between adsorbent and Cr(VI).

The Langmuir isotherm model assumed that the adsorption process was monolayer sorption on a homogeneous sorption surface, and all the sorption sites were equal and finite, while the Freundlich isotherm model was an empirical equation for explaining heterogeneous adsorption process.³³ Both the two models were expressed as follows:

$$\text{Langmuir: } q_e = \frac{q_m K_L c_e}{1 + K_L c_e} \quad (2)$$

$$R_L = \frac{1}{1 + K_L c_0} \quad (3)$$

$$\text{Freundlich: } q_e = K_F c_e^{1/n} \quad (4)$$

where c_e is the equilibrium concentration (mg L^{-1}), c_0 is the initial concentration (mg L^{-1}), q_e is the amount of Cr(VI) adsorbed at equilibrium (mg g^{-1}), q_m is the maximum adsorption capacity (mg g^{-1}), R_L is the separation factor of the Langmuir. K_L is the Langmuir constant related to the affinity of the binding sites (L mg^{-1}), and K_F and n are the Freundlich constants related to the adsorption capacity and intensity, respectively.

The related parameters of the two models were listed in Table 2. It indicated that the correlation coefficient R^2 of Langmuir was higher than that of Freundlich, which suggested that the adsorption process of Cr(VI) onto CMB fit the Langmuir model better than Freundlich model. Moreover, from the equation above we can see that $0 < R_L < 1$ obviously, which manifested that the adsorption in this research was suitable for Langmuir model more adequately. It indicated that monolayer adsorption and heterogeneous surface conditions might coexist under the experimental conditions, but monolayer adsorption was more dominant.²⁴ Fig. 9 showed that the q_m increased with the increasing of the temperature. The values of the q_m were 151.62, 157.11, 167.31 mg g^{-1} , which was corresponding to 20, 30, 40 °C. In addition, K_L increased with the increasing of the temperature. Therefore, the adsorption process of Cr(VI) onto CMB is endothermic.²⁸ Comparing the maximum capacity of Cr(VI) removal with the previous study³⁴⁻³⁸ (shown in Table 3), CMB was better than many other absorbents reported in the literature.

3203.4 Thermodynamic analysis

321 Thermodynamic analysis was considered to gain an in-depth study of the
322adsorption process of Cr(VI) onto CMB. Thermodynamic parameters such as Gibbs
323free energy ΔG^0 , enthalpy ΔH^0 , entropy ΔS^0 were calculated by the following
324equations:

$$325 \Delta G^0 = -RT \ln K \quad (5)$$

$$326 \ln K = -\frac{\Delta G^0}{RT} = -\frac{\Delta H^0}{RT} + \frac{\Delta S^0}{R} \quad (6)$$

327where K is the adsorption equilibrium constant. T (K) is the absolute temperature, and
328 R ($8.314 \text{ J mol}^{-1} \text{ K}^{-1}$) is the gas constant. ΔH^0 and ΔS^0 could be calculated from the
329slope and intercept of $\ln K$ versus $1/T$. The results of the thermodynamic parameters
330were shown in Table 4.

331 From Table 4, we can see that the negative values of the ΔG^0 ($-19.97 \text{ kJ mol}^{-1}$ at
332293.15 K, $-20.82 \text{ kJ mol}^{-1}$ at 303.15 K, and $-21.59 \text{ kJ mol}^{-1}$ at 313.15 K) became
333more negative with the rising temperature, which indicated that the process of the
334adsorption was spontaneous in nature and the degree of the reaction spontaneity
335increased with the rising temperature.²⁴ Furthermore, the positive value of ΔH^0 (3.67
336 kJ mol^{-1}) demonstrated that the sorption was endothermic, which was consistent with
337the result of the adsorption isotherm. Finally, the positive value of ΔS^0 (80.68 J
338 $\text{K}^{-1}\text{mol}^{-1}$) probably reflected the growth of randomness at the solid/solution interface
339during the adsorption process and a good affinity of Cr(VI) onto CMB.²⁴ Moreover,
340some structural changes of adsorbate and adsorbent may also occur during the

adsorption process. In conclusion, the sorption of Cr(VI) onto CMB is an endothermic and spontaneous process.

3.5 Kinetic studies

The effect of the contact time on CMB adsorption capacity was shown in Fig. 10(a). The removal capacity of CMB on Cr(VI) markedly increased in the first 120 min, which was owing to the existence of plentiful active sites on the adsorbent surface. And then, the trend rose slowly until the adsorption equilibrium was reached within 360 min. The reason for the slow adsorption process was that the majority of active surface sites were occupied by Cr(VI), and there were insufficient binding sites for the material adsorbing Cr(VI).

To investigate the mechanism of adsorption, kinetic models were applied to explain the experimental data. In this research, two different models were applied and illustrated as follows:

The pseudo-first-order model:

$$\log(q_e - q_t) = \log q_e - \frac{k_1}{2.303} t \quad (7)$$

The pseudo-second-order model:

$$\frac{t}{q_t} = \frac{t}{q_e} + \frac{1}{k_2 q_e^2} \quad (8)$$

where q_e and q_t are the adsorption amounts (mg g^{-1}) at equilibrium and at time t , respectively. k_1 is the pseudo-first-order rate constant (min^{-1}), k_2 is the pseudo-second-order rate constant ($\text{g mg}^{-1} \text{min}^{-1}$).

Contact time effect and pseudo-second-order sorption kinetics were shown in

Fig. 10 (a) and (b), respectively. The kinetic parameters calculated from the two models were listed in Table 5. Obviously, the correlation coefficient R^2 of the pseudo-second-order model was more than 0.99, which was higher than that of the pseudo-first-order model. Besides, the calculated q_e agreed very well with the experimental data. The result indicated that the kinetic data for the adsorption process fit the pseudo-second-order model, which showed that the mechanism of Cr(VI) sorption by the CMB depended on the rate-controlling step due to chemical sorption.^{28, 39, 40}

3.6 Effect of background electrolyte on Cr(VI) removal

Fig. 11 showed the effect of background electrolyte on the Cr(VI) adsorption onto the CMB at pH 2 in 0.01 mol L⁻¹ NaCl, Ca(NO₃)₂, CaCl₂, Na₃PO₄, Na₂SO₄ solution, respectively. As shown in Fig. 11, all the five electrolyte have the influence of different levels, which is reflected by the following sequence of the Cr(VI) sorption capacity: NaCl > Ca(NO₃)₂ > CaCl₂ > Na₃PO₄ > Na₂SO₄. NaCl, Ca(NO₃)₂ and CaCl₂ had less effect on the removal of Cr(VI) than the other two electrolytes. Na₃PO₄ and Na₂SO₄ inhibited the Cr(VI) sorption distinctly and reduced the adsorption capacity from 108.84 mg g⁻¹ to 63.17 mg g⁻¹, 47.49 mg g⁻¹, respectively. What can explain this phenomenon is the competition mechanism. As for NaCl, Ca(NO₃)₂, CaCl₂, Cl⁻ and NO₃⁻ are monovalent anions, and they may slightly compete with the chromium anion for the positive charge sorption sites on the CMB surface. However, the PO₄³⁻ and the SO₄²⁻ from Na₃PO₄ and Na₂SO₄ are multivalent anions, which could compete with Cr₂O₇²⁻, HCrO₄⁻, KCrO₄⁻, CrO₄²⁻ for more available sorption sites of the CMB. The

study of the effect of background electrolyte on Cr(VI) removal demonstrated that electrostatic force is one possible sorption mechanism for the removal of Cr(VI) onto CMB.

4. Conclusions

In this work, chitosan-biochar/ γ -Fe₂O₃ was successfully synthesized and applied to remove Cr(VI) from the wastewater. The magnetic composite possessed a high Cr(VI) adsorption capacity and can be easily separated from the solution, by combining the superiority of chitosan, biochar and γ -Fe₂O₃. The features of the novel material were low operating cost, easily available biomass resource, magnetic, abundant functional groups, and the remission of the invasive species (*Eichhornia crassipes*). Moreover, The adsorption capacity was affected by the solution pH and the maximum Cr(VI) adsorption capacity was found at pH 2. The Langmuir isotherm model fit the experimental data very well. It indicated that monolayer adsorption is the main mechanism. The maximum adsorption capacity obtained from Langmuir model were 139.21, 154.37 and 164.71 mg g⁻¹ at 20, 30 and 40 °C, respectively. Kinetic studies showed that the pseudo-second-order model illustrated the best description for the adsorption process of Cr(VI) onto CMB, which suggested the rate limiting step may be chemisorption. The analysis of thermodynamic showed that the sorption of Cr(VI) onto CMB was an endothermic and spontaneous process. Cr(VI) adsorption can be restrained by some multivalent anions, such as PO₄³⁻ and SO₄²⁻. Moreover, the FTIR and XPS analysis illustrated that the functional groups changed

404after modification, resulting in enhancing the sorption ability for Cr(VI). In
405conclusion, the effective and environmental friendly absorbent (CMB) will have
406broad applications in the removal of Cr(VI) from wastewater.

407Acknowledgements

408 The authors would like to thank financial support from the National Natural
409Science Foundation of China (Grant No. 41271332, 51478470 and 51108167).

410References

4111. L. Tang, G.-D. Yang, G.-M. Zeng, Y. Cai, S.-S. Li, Y.-Y. Zhou, Y. Pang, Y.-Y. Liu, Y. Zhang
412 and B. Luna, *Chem. Eng. J.*, 2014, 239, 114-122.
4132. Y. S. Shen, S. L. Wang, Y. M. Tzou, Y. Y. Yan and W. H. Kuan, *Bioresour. Technol.*, 2012, 104,
414 165-172.
4153. Q. Zhou and Y. Song, Beijing: Science Press, 2004.
4164. X. Zhou, T. Korenaga, T. Takahashi, T. Moriwake and S. Shinoda, *Water. Res.*, 1993, 27,
417 1049-1054.
4185. Y. Pang, G.-M. Zeng, L. Tang, Y. Zhang, Y.-Y. Liu, X.-X. Lei, M.-S. Wu, Z. Li and C. Liu,
419 *Bioresour. Technol.*, 2011, 102, 10733-10736.
4206. D. Mohan and C. U. Pittman Jr, *J. Hazard. Mater.*, 2006, 137, 762-811.
4217. Y. A. Aydin and N. D. Aksoy, *Chem. Eng. J.*, 2009, 151, 188-194.
4228. P. Xu, G. M. Zeng, D. L. Huang, C. L. Feng, S. Hu, M. H. Zhao, C. Lai, Z. Wei, C. Huang, G.
423 X. Xie and Z. F. Liu, *Sci. Total Environ.*, 2012, 424, 1-10.
4249. F. Zhang, X. Wang, D. Yin, B. Peng, C. Tan, Y. Liu, X. Tan and S. Wu, *J. Environ. Manage.*,

- 425 2015, 153, 68-73.
42610. Y. Huang, S. Li, J. Chen, X. Zhang and Y. Chen, *Appl. Surf. Sci.*, 2014, 293, 160-168.
42711. I. Guerrero-Coronilla, L. Morales-Barrera and E. Cristiani-Urbina, *J. Environ. Manage.*, 2015,
- 428 152, 99-108.
42912. M. Zhang, B. Gao, Y. Yao, Y. Xue and M. Inyang, *Sci. Total Environ.*, 2012, 435-436, 567-
- 430 572.
43113. Y. Yao, B. Gao, H. Chen, L. Jiang, M. Inyang, A. R. Zimmerman, X. Cao, L. Yang, Y. Xue and
- 432 H. Li, *J. Hazard. Mater.*, 2012, 209-210, 408-413.
43314. X. F. Tan, Y. G. Liu, G. M. Zeng, X. Wang, X. J. Hu, Y. L. Gu and Z. Z. Yang, *Chemosphere*,
- 434 2015, 125, 70-85.
43515. Y. Zhou, B. Gao, A. R. Zimmerman, J. Fang, Y. Sun and X. Cao, *Chem. Eng. J.*, 2013, 231,
- 436 512-518.
43716. Y. Xue, B. Gao, Y. Yao, M. Inyang, M. Zhang, A. R. Zimmerman and K. S. Ro, *Chem. Eng. J.*,
- 438 2012, 200-202, 673-680.
43917. M. Zhang, B. Gao, Y. Yao, Y. Xue and M. Inyang, *Sci. Total Environ.*, 2012, 435-436, 567-
- 440 572.
44118. W. Zhang, L. Wang and H. Sun, *Chemosphere*, 2011, 85, 1306-1311.
44219. D. Kołodyńska, *Chem. Eng. J.*, 2011, 173, 520-529.
44320. T. PHENRAT, Y. LIU, R. D. TILTON and G. V. LOWRY, *Environ. Sci. Technol.*, 2008, 43,
- 444 1507-1514.
44521. Y. Pang, G. Zeng, L. Tang, Y. Zhang, Y. Liu, X. Lei, Z. Li, J. Zhang, Z. Liu and Y. Xiong,
- 446 *Chem. Eng. J.*, 2011, 175, 222-227.
44722. M. Zhang, B. Gao, S. Varnoosfaderani, A. Hebard, Y. Yao and M. Inyang, *Bioresour. Technol.*,
- 448 2013, 130, 457-462.

44923. B. Chen, Z. Chen and S. Lv, *Bioresour. Technol.*, 2011, 102, 716-723.
45024. T.-t. Li, Y.-g. Liu, Q.-q. Peng, X.-j. Hu, T. Liao, H. Wang and M. Lu *Chem. Eng. J.*, 2013, 214, 189-197.
45225. Y. Ren, H. A. Abboud, F. He, H. Peng and K. Huang, *Chem. Eng. J.*, 2013, 226, 300-311.
45326. X. Dong, L. Q. Ma and Y. Li, *J. Hazard. Mater.*, 2011, 190, 909-915.
45427. S. Hou, S. Su, M. L. Kasner, P. Shah, K. Patel and C. J. Madarang, *Chem. Phys. Lett.*, 2010, 501, 68-74.
45628. H. Wang, Y. G. Liu, G. M. Zeng, X. J. Hu, X. Hu, T. T. Li, H. Y. Li, Y. Q. Wang and L. H. Jiang, *Carbohydr. Polym.*, 2014, 113, 166-173.
45829. Changsheng Shan, Huafeng Yang, Dongxue Han, Qixian Zhang, Ari Ivaska and L. Niu, *Langmuir*, 2009, 25, 12030-12033.
46030. L. Q. Xu, D. Wan, H. F. Gong, K. G. Neoh, E. T. Kang and G. D. Fu, *Langmuir*, 2010, 26, 15376-15382.
46231. Q. Cheng, C. Li, L. Xu, J. Li and M. Zhai, *Chem. Eng. J.*, 2011, 173, 42-48.
46332. T. Chen, Y. Zhang, H. Wang, W. Lu, Z. Zhou, Y. Zhang and L. Ren, *Bioresour. Technol.*, 2014, 164, 47-54.
46533. X. J. Hu, J. S. Wang, Y. G. Liu, X. Li, G. M. Zeng, Z. L. Bao, X. X. Zeng, A. W. Chen and F. Long, *J. Hazard. Mater.*, 2011, 185, 306-314.
46734. A. K. Giri, R. Patel and S. Mandal, *Chem. Eng. J.*, 2012, 185-186, 71-81.
46835. S. Nethaji, A. Sivasamy and A. B. Mandal, *Bioresour. Technol.*, 2013, 134, 94-100.
46936. E. A. Oliveira, S. F. Montanher, A. D. Andrade, J. A. Nóbrega and M. C. Rollemberg, *Process Biochem.*, 2005, 40, 3485-3490.
47137. A. Rao, A. Bankar, A. R. Kumar, S. Gosavi and S. Zinjarde, *J. Contam. Hydrol.*, 2013, 146, 63-73.

47338. N. N. Thinh, P. T. Hanh, T. T. Ha le, N. Anh le, T. V. Hoang, V. D. Hoang, H. Dang le, N. V.
474 Khoi and T. D. Lam, *Mater. Sci. Eng., C, Mater. Biol. Appl.*, 2013, 33, 1214-1218.
47539. D. Kołodyńska, R. Wnętrzak, J. J. Leahy, M. H. B. Hayes, W. Kwapiński and Z. Hubicki,
476 *Chem. Eng. J.*, 2012, 197, 295-305.
47740. Z. Sun, Y. Liu, Y. Huang, X. Tan, G. Zeng, X. Hu and Z. Yang, *J. Colloid Interface Sci.*, 2014,
478 434, 152-158.

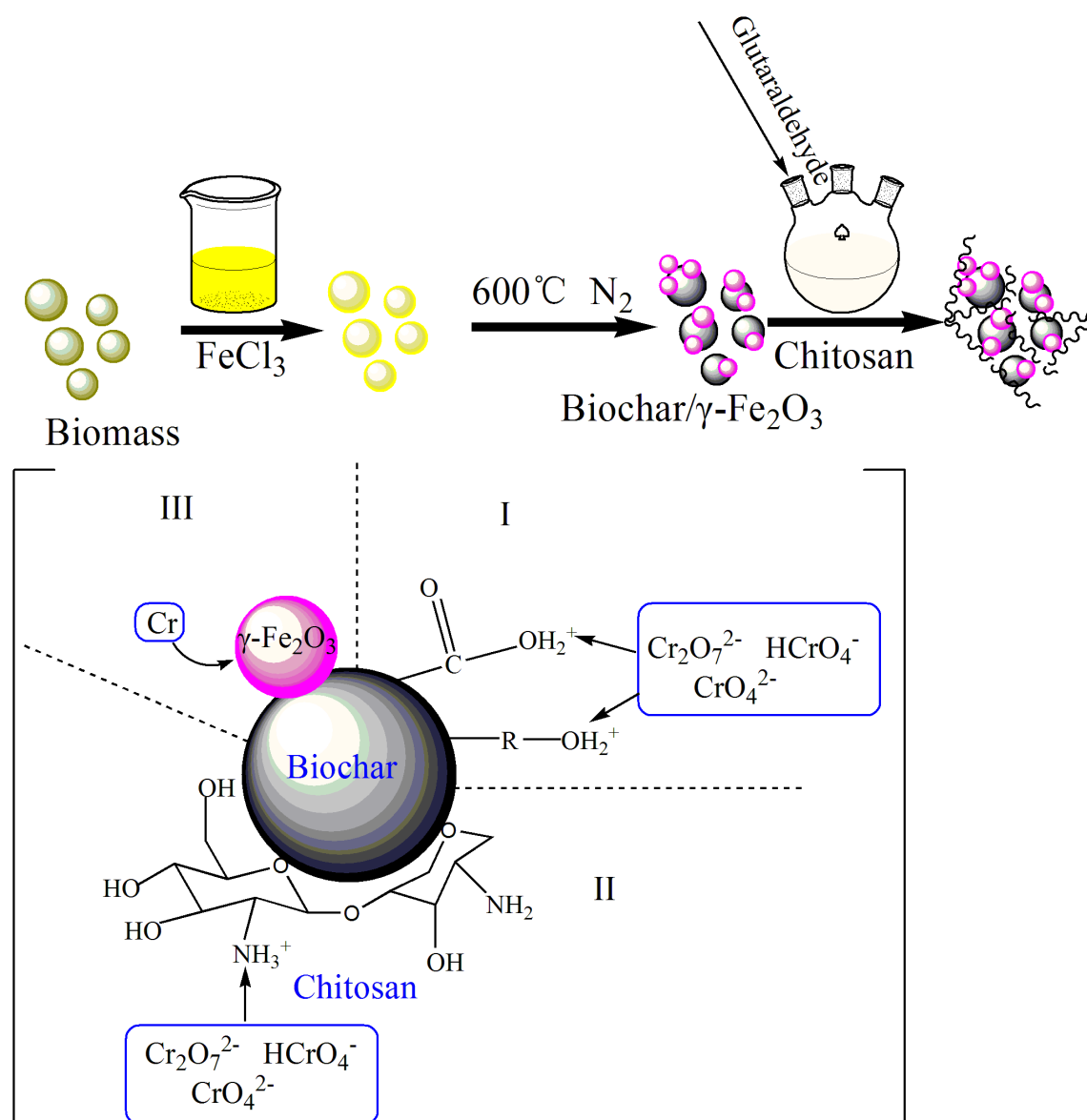


Fig. 1. Schematic representation of strategy for preparation of CMB and Cr(VI) removal by CMB.

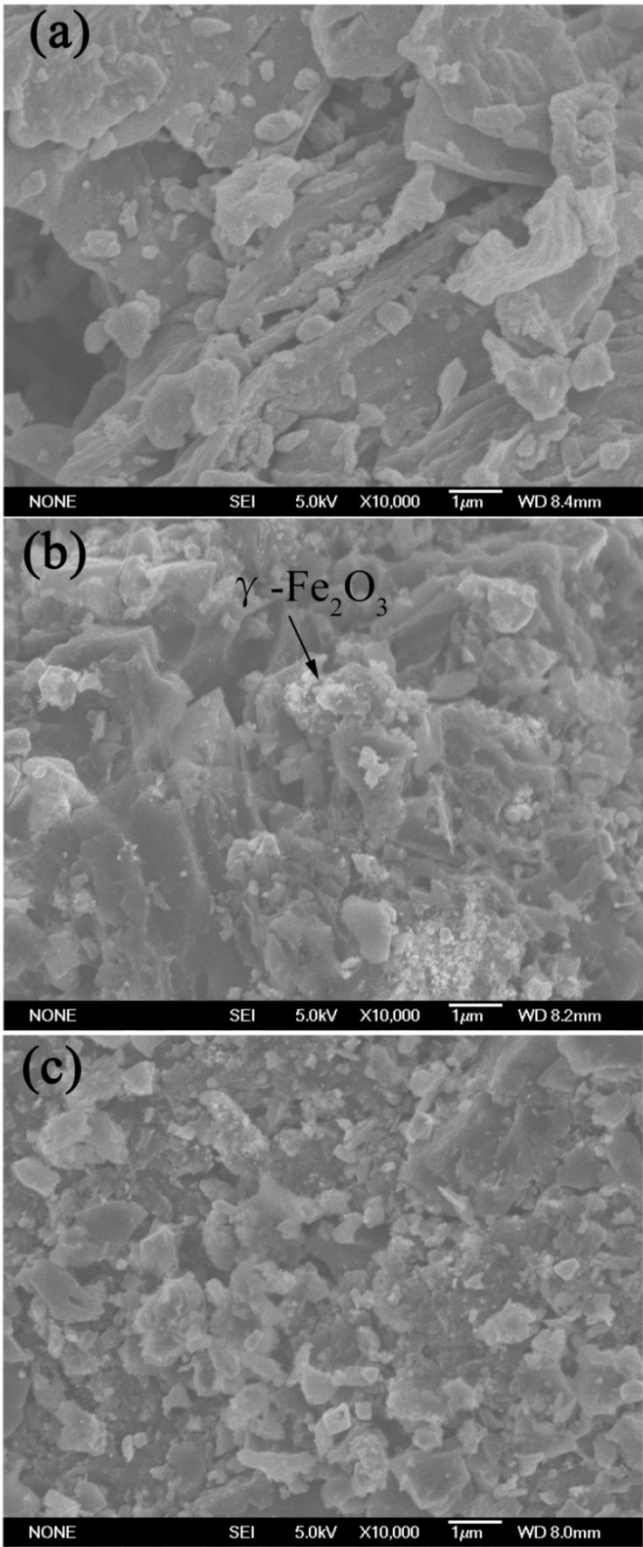


Fig. 2. SEM images of pristine biochar (a), MB (b) and CMB (c).

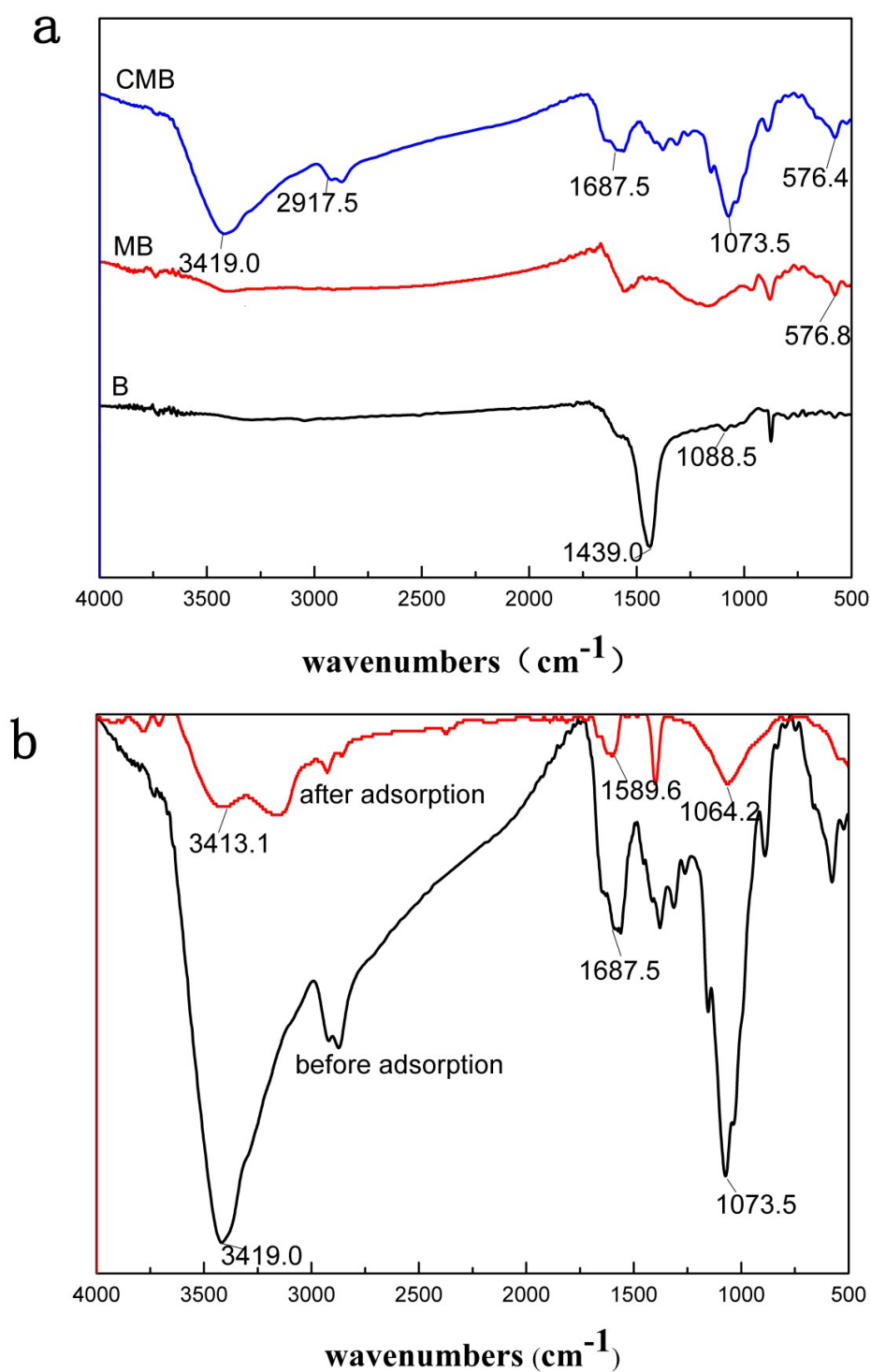


Fig. 3. (a) FTIR spectra of B, MB and CMB, (b) FTIR spectra of CMB before and after adsorption

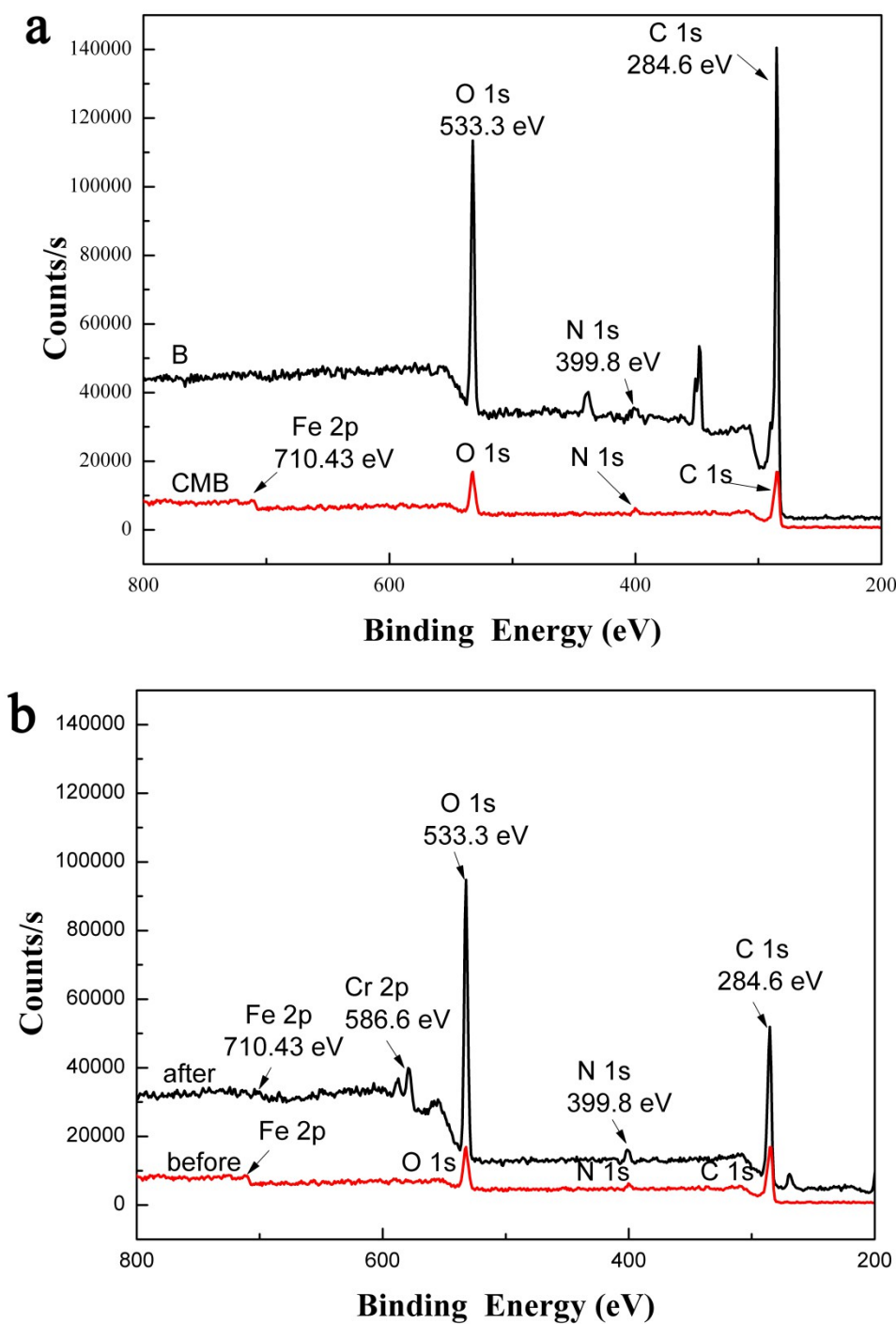


Fig. 4. (a) XPS survey spectra of B and CMB, (b) XPS survey spectra of CMB before and after adsorption

Fig. 5. The C 1s XPS spectra of B (a), CMB (b), CMB after adsorption (c).

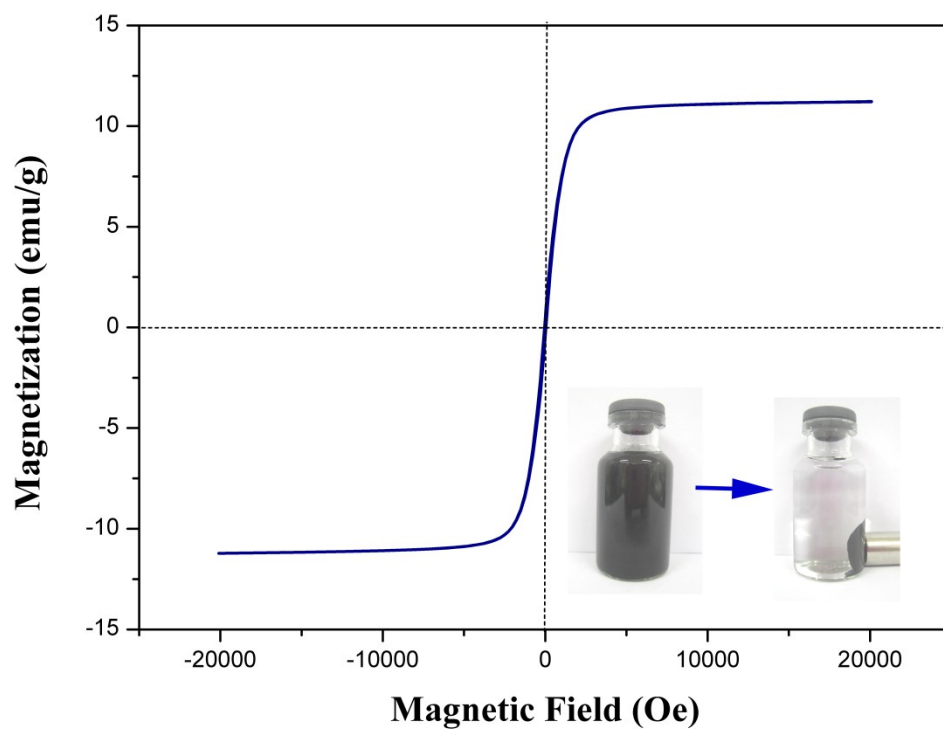


Fig. 6. Magnetization curve of CMB at room temperature (the insets show the CMB dispersed in ultrapure water and the magnetic separation)

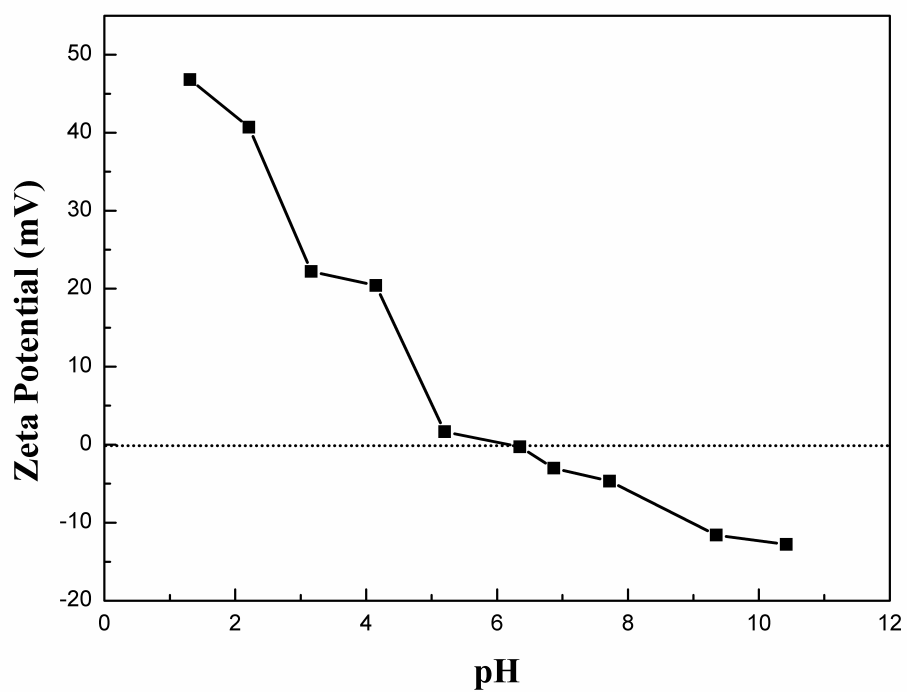


Fig. 7. Zeta potential of CMB at different solution pH.

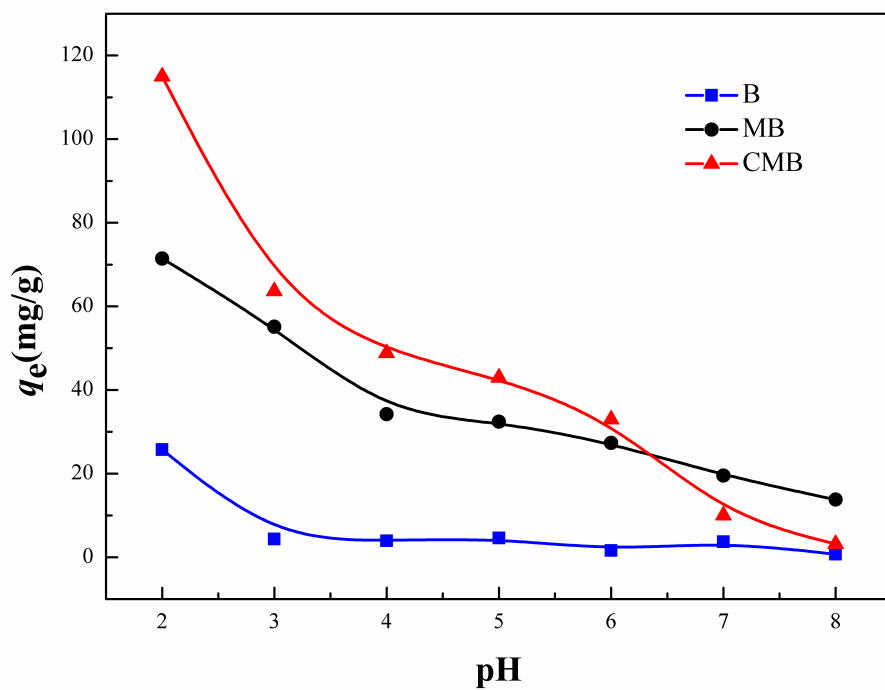


Fig. 8. Effect of the initial solution pH on adsorption of Cr(VI) by B, MB and CMB

(Reaction conditions: $c_0 = 150 \text{ mg L}^{-1}$; $V = 50 \text{ mL}$; $m = 50 \text{ mg}$; $t = 6 \text{ h}$; $T = 30 \text{ }^\circ\text{C}$).

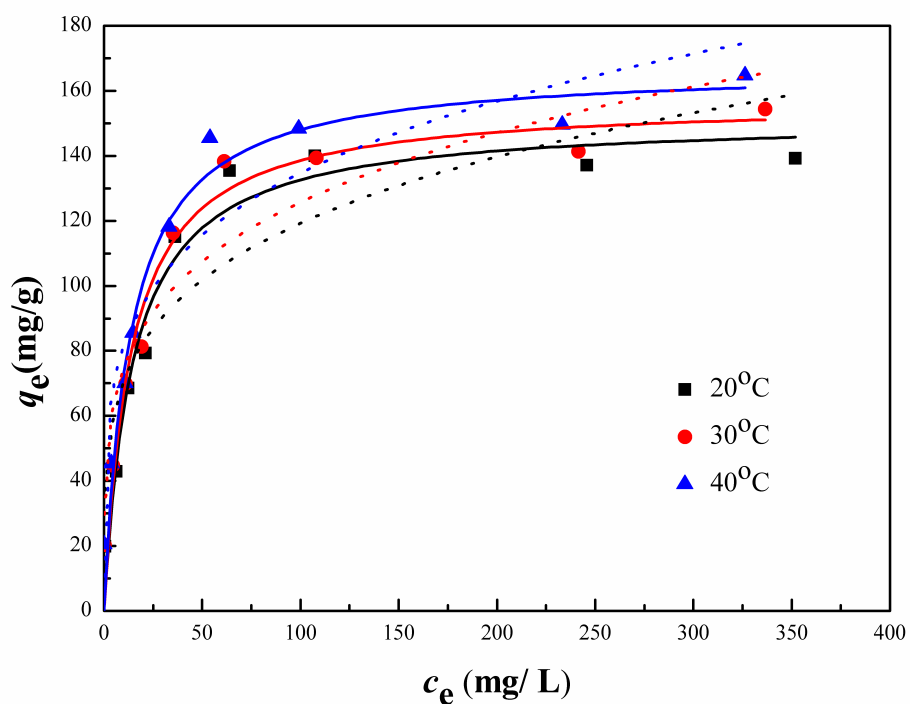


Fig. 9. Langmuir isotherm (solid line) and Freundlich isotherm (dash line) for the adsorption of Cr(VI) on CMB (Reaction conditions: $c_0 = 20\text{-}500\text{ mg L}^{-1}$; $V = 50\text{ mL}$; $m = 50\text{ mg}$; $t = 6\text{ h}$; $\text{pH} = 2$; $T = 20, 30, 40\text{ }^\circ\text{C}$).

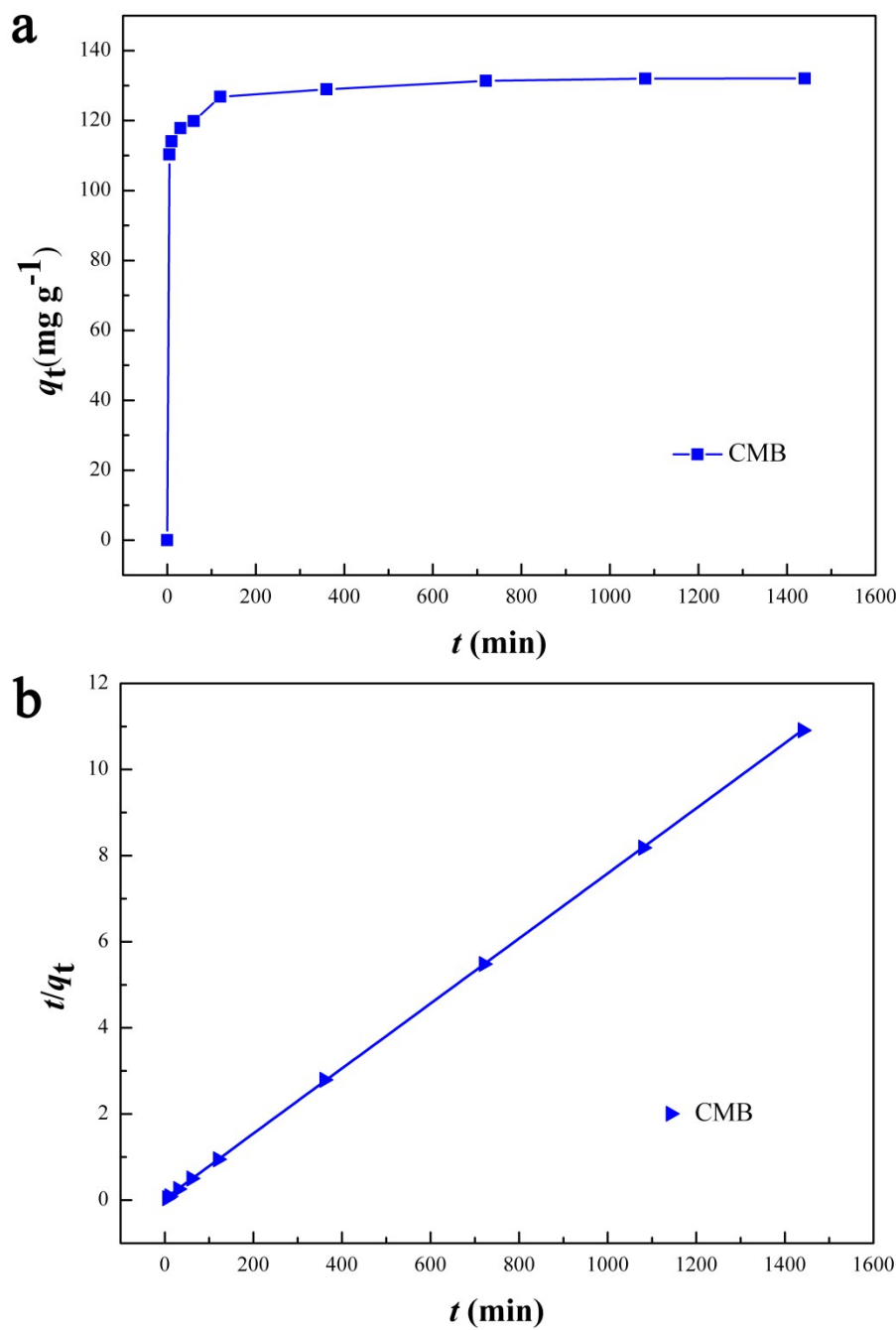


Fig. 10. (a) Effect of contact time of Cr(VI) adsorption onto CMB and (b) pseudo-second-order sorption kinetics of Cr(VI) adsorption onto CMB (Reaction conditions: $c_0 =$

200 mg L⁻¹; $V = 50$ mL; $m = 50$ mg; pH = 2; T = 30 °C).

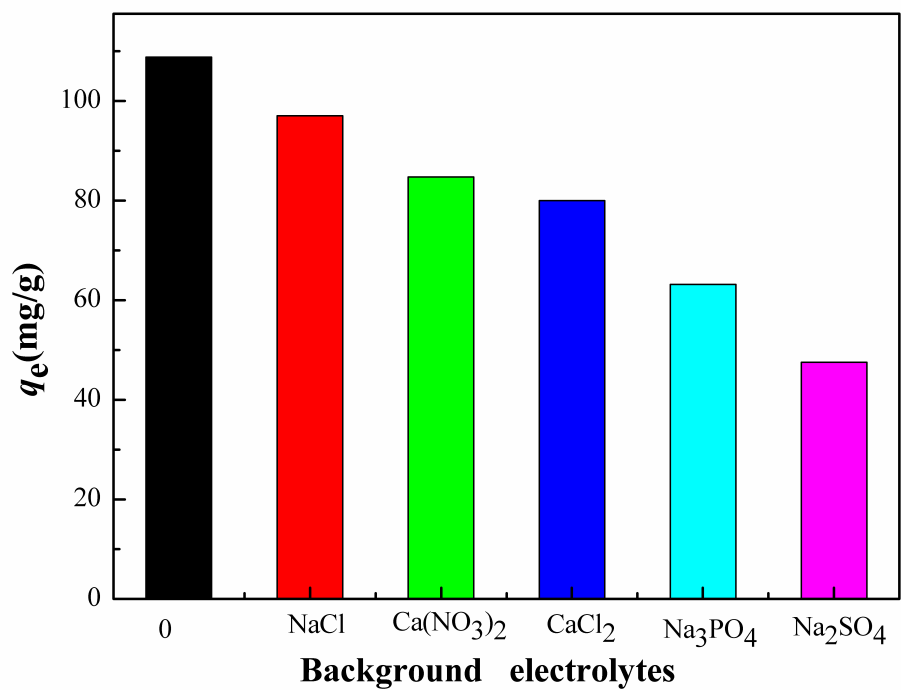


Fig. 11. Effect of background electrolyte (NaCl, Ca(NO₃)₂, CaCl₂, Na₃PO₄, Na₂SO₄) on the Cr(VI) adsorption by CMB. (Reaction conditions: electrolyte concentration 0.01 mol L⁻¹; Cr(VI) concentration $c_0 = 150 \text{ mg L}^{-1}$; $V = 50 \text{ mL}$; $m = 50 \text{ mg}$; $T = 30 \text{ }^\circ\text{C}$; pH = 2).

Table 1.

Pore distribution properties of the three materials

	BET surface area (m ² g ⁻¹)	Pore volume (m ³ g ⁻¹) ^a	Pore size (nm) ^b
B	37.68	0.055	5.86
MB	341.09	0.20	2.36
CMB	90.78	0.064	2.81

^a Determined at $P/P_0 = 0.99$ ^b Adsorption average pore width (4V/A by BET).

Table 2.

Adsorption equilibrium constants obtained from Langmuir and Freundlich isotherms in the adsorption of Cr(VI) onto CMB.

Temperature (°C)	Langmuir			Freundlich		
	q_{max} (mg g ⁻¹)	K_L (L mg ⁻¹)	R^2	K_F (L mg ⁻¹)	n	R^2
20	151.62	0.069	0.95	41.74	4.37	0.81
30	157.11	0.074	0.96	44.36	4.42	0.88
40	167.31	0.077	0.96	49.05	4.56	0.87

Table 3.

Comparison of the maximum Cr(VI) adsorption capacity (q_m) of various adsorbents.

Adsorbents	q_m (mg g ⁻¹)	References
Activated carbon derived from <i>Eichhornia crassipes</i> root biomass	36.34	34
Magnetized activated carbon	57.19	35
Saw dust activated carbon	65.8	36
Fe ⁰ /Fe ₃ O ₄ nanoparticles	55.64	37
Magnetic chitosan 2 (NCIM 3590)	137.27	38
Chitosan-biochar/ γ -Fe ₂ O ₃ composite (CMB)	167.31	This study

Table 4.

Thermodynamic parameters for the adsorption of Cr(VI) by CMB

ΔH^0 (kJ mol ⁻¹)	ΔS^0 (J K ⁻¹ mol ⁻¹)	ΔG^0 (kJ mol ⁻¹)		
		20 °C	30 °C	40 °C
3.67	80.68	-19.97	-20.82	-21.59

Table 5.

Pseudo-first-order model and pseudo-second-order model parameters for Cr(VI) adsorption on CMB.

Pseudo-first-order model			Pseudo-second-order model		
k_1 (min^{-1})	q_e (mg g^{-1})	R^2	k_2 ($\text{g mg}^{-1} \text{min}^{-1}$)	q_e (mg g^{-1})	R^2
4.71×10^{-4}	31.95	0.65	1.74×10^{-4}	132.28	0.99